Fluid Control in Multichannel Structures by Electrocapillary Pressure

M. W. J. Prins,* W. J. J. Welters, J. W. Weekamp

We demonstrate control of fluid motion in three-dimensional structures with thousands of microchannels. Fluids are manipulated via an electrocapillary pressure, originating from electrostatic control of the solid/fluid interfacial tension in the microchannels. Reversible fluid displacement has been achieved for all channel orientations with respect to gravity. The velocities of several centimeters per second are nearly two orders of magnitude higher than the velocities demonstrated by other electrofluidic actuation principles.

Fluids play an essential role in many processes and applications, ranging from (bio)chemical synthesis and analysis, to liquid-crystal displays, printing technologies, and techniques to manipulate solid components. With the rapid advances in microfabrication technologies, challenges have arisen to develop miniaturized fluidic devices with a large number of channels or cells. In order to achieve control of the position and velocity of fluids in a structure with many thousands of microchannels, it is essential to develop integrated actuation principles that can operate locally on the fluids. Ideally, the actuation principle does not involve moving parts, is scalable to micrometer sizes, and is electrically controlled, rapid, reversible, and of low power consumption. Recently, nonmechanical electrofluidic manipulation was demonstrated with redox-active surfactants (*1*) and by electro-osmotic flow (*2*). The maximum flow velocities that have been demonstrated with these techniques are of the order of millimeters per second. We present fluid actuation by an electrocapillary pressure (ECP) originating from electrostatic control of the solid/fluid interfacial tension in a microchannel. Micropumping by electrocapillary effects has been proposed in a theoretical study (*3*). Recent experimental work on electrostatic control of solid/fluid interfacial tension focused on planar and droplet geometries (*4*–*7*). We demonstrate experimentally that ECP allows highly reversible fluid displacement at velocities of several centimeters per second, in three-dimensional structures with many thousands of microchannels.

The basic component of our experiment (Fig. 1A) is a microchannel with electrodes inside the walls. The microchannel is filled with two fluids that are immiscible and have different electrical conductivities. For example, one fluid is an aqueous solution (electrically conducting) whereas the other fluid is a gas or a nonpolar oil (electrically insulating). When the channel is of submillimeter diameter, internal capillary effects are important. The capillary pressure on the fluid/fluid meniscus is determined by the difference between two interfacial tensions, namely the tension of the interface between the wall and the conducting fluid versus the tension of the interface between the wall and the insulating fluid. To be able to control the fluid flow, we exploit the phenomenon of electrocapillarity, i.e., the fact that the apparent interfacial tension depends on the electrical charge density accumulated at the interface (*8*, *9*). The charge distribution (Fig. 1B) is shown when a voltage is applied between the aqueous solution and the electrode. Due to the electrostatic attraction between the fluidic charge and its image charge in the electrode, the energy of the interface between the conducting fluid and the channel wall is reduced and the wetting of the microchannel wall by the conducting fluid is enhanced. The charge-induced reduction of interfacial tension $\Delta\gamma$ equals $d{\cdot}\sigma^2/2\varepsilon_0\varepsilon_r$, where d is the thickness of the insulating layer, σ the net charge density accumulated in the aqueous solution, and ε_r the dielectric constant of the insulator (*5*). Using Gauss' law ($\sigma = \varepsilon_0\varepsilon_r V/d$) we find $\Delta\gamma = \varepsilon_0\varepsilon_r V^2/2d$ (*4*), with V the voltage applied to the microchannel electrode. The ability to modify the interfacial tension inside a microchannel gives an electrical tuning range of the pressure generated by the meniscus, an electrocapillary pressure (*10*)

$$\mathrm{ECP} = \frac{\text{force}}{\text{area}} = \frac{\ell\Delta\gamma}{A} = \frac{\ell}{A}\,\frac{1}{2}\,\frac{\varepsilon_0\varepsilon_r}{d}V^2 \qquad (1)$$

This equation applies for a microchannel with an arbitrary shape, ℓ being the inner circumference of the channel and A the cross-sectional area of the channel. The charge-induced pressure contribution is always positive, promoting the influx of the conducting fluid into the channel. The size of the ECP is given by the channel geometry (ℓ/A) and by the electrostatic energy density at the interface between the conducting fluid and the channel wall. For a cylindrical channel, the ECP equals $2\Delta\gamma/R$, with R the channel radius. Because the magnitude of the ECP is inversely proportional to the channel radius, the actuation mechanism is well suited for small-scale devices.

To investigate fluid control by ECP, we employed multichannel structures with honeycomb-shaped microchannels (*11*), with ev-

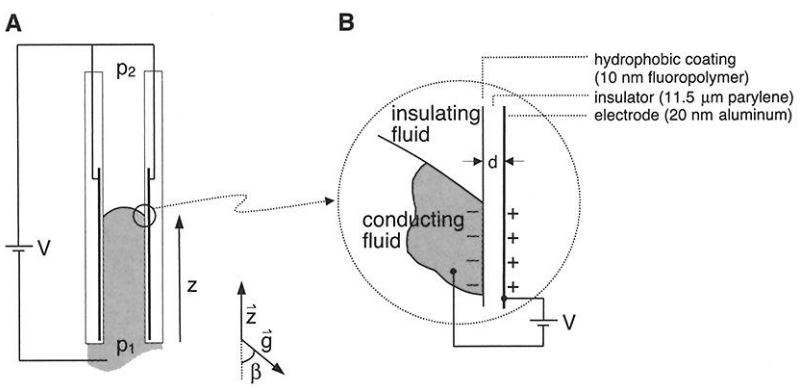

Fig. 1. (**A**) Sketch of fluid in a microchannel. The fluid at the bottom (shown in gray) is electrically conducting (an aqueous salt solution was used in our experiments). The top contains an insulating fluid (either air or a nonpolar oil in our experiments). A voltage V is applied to the electrode; the aqueous solution is at ground potential. The pressures at the bottom and top openings of the microchannel are expressed as p_1 and p_2, respectively. The angle between the gravitational force and the long axis of the microchannel is given by β. (**B**) Close-up of the meniscus edge. Inside the microchannel wall, a 20-nm-thick aluminum electrode is present, separated from the aqueous solution by an insulating layer of thickness d. The insulating layer consists of an 11.5-μm thickness of parylene (deposited by chemical vapor polymerization of di-*p*-xylylene) with a 10-nm fluoropolymer coating (AF1600 of DuPont, deposited from solution). Because of the applied electric field, opposite charge densities are induced at the fluid/solid interface and in the subsurface electrode. The electrostatic attraction between the aqueous solution and the electrode enhances the coverage of the wall by the aqueous solution.

Philips Research Eindhoven, Prof. Holstlaan 4, NL-5656 AA Eindhoven, Netherlands.

*To whom correspondence should be addressed. E-mail: menno.prins@philips.com

ery microchannel having a diameter of about 350 μm. A top view of a number of microchannels is shown (Fig. 2A). The microchannel walls are coated with an aluminum electrode and capped by an insulating coating with hydrophobic properties. The flow of fluid into or out of the microchannels is mediated by communication channels (Fig. 2B). For a direct demonstration of ECP, we measured the voltage dependence of the pressure generated by the menisci. First, an external hydrostatic pressure was applied to push the aqueous solution into the hydrophobic microchannels; subsequently, the external valves were closed. Figure 2C shows the voltage-induced contribution to the pressure generated by the menisci. Hysteresis and drift are insignificant in the data. The experimental results are in very good agreement with Eq. 1, a direct proof of ECP.

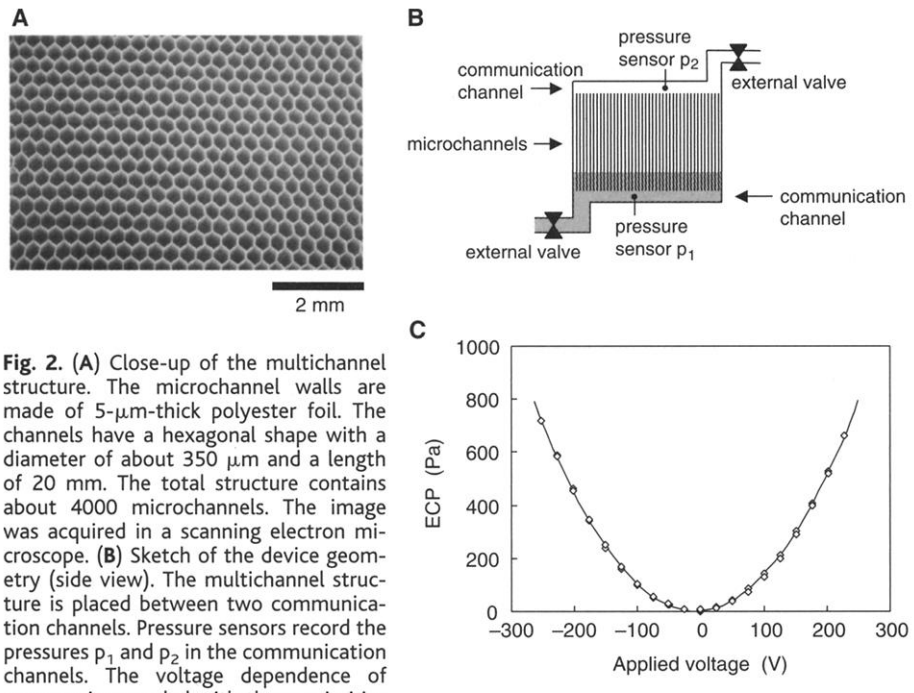

Fig. 2. (**A**) Close-up of the multichannel structure. The microchannel walls are made of 5-μm-thick polyester foil. The channels have a hexagonal shape with a diameter of about 350 μm and a length of 20 mm. The total structure contains about 4000 microchannels. The image was acquired in a scanning electron microscope. (**B**) Sketch of the device geometry (side view). The multichannel structure is placed between two communication channels. Pressure sensors record the pressures p_1 and p_2 in the communication channels. The voltage dependence of pressure is recorded with the menisci inside the microchannels and the external valves closed. All microchannel electrodes are activated with the same voltage V; the aqueous solution is at ground potential. (**C**) ECP as a function of applied voltage. Symbols represent measured values, using the voltage sweep 0/−227/0/+227/0/−252 V. The solid line represents the theoretical behavior according to Eq. 1, in agreement with the independently measured parameters $A = 0.12 \pm 0.01$ mm^2, $\ell = 1.29 \pm 0.05$ mm, $\varepsilon_r = 2.7$, and $d = 11.5 \pm 0.5$ μm. The minimum of the parabola is located at −7 V.

The electrostatic forces on the meniscus can be used to position fluids in microchannels. Figure 3 illustrates the filling and emptying characteristics of a multichannel structure. The external valves were open to maintain constant pressures in the communication channels. The filling and emptying of microchannels can be visualized in an x-ray transmission image, due to the high x-ray transparency of the microchannel walls. Figure 3A shows a multichannel structure in side view. The aqueous solution has been made to absorb x-rays by the addition of CsCl. At the bottom of the panels (Fig. 3A), the aqueous communication channel is visible. External electrical contacts serve to apply voltages to the aluminum electrodes in single microchannels or to clusters of microchannels. In this particular device, eight external contacts are visible at the top of the x-ray images, each contact connected to a cluster of microchannels six or seven microchannels in width. In the left image, all electrodes are at ground potential, causing the microchannels to be empty of aqueous solution. In the right image, an external contact has been activated, causing one cluster of microchannels to visibly fill with aqueous solution. The microchannels fill to a level of 10 mm, determined by the length of the aluminum pattern in the microchannels.

The filling and emptying behavior is characterized further as a function of the applied

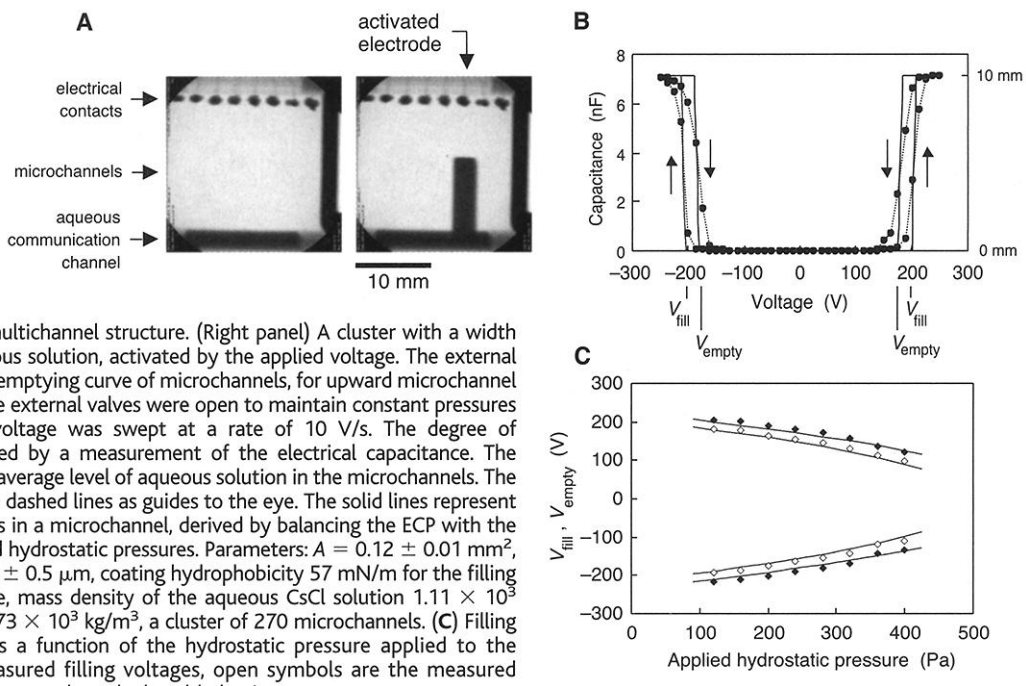

Fig. 3. (**A**) Transmission x-ray images of a multichannel device (side view). The pictures were taken with the x-rays oriented perpendicular to the microchannel axes. The aqueous solution shows high x-ray contrast due to the added CsCl salt. The microchannel walls are highly transparent to x-rays. At the bottom of the pictures, the communication channel for aqueous solution is visible. A series of eight external electrical contacts is apparent at the top of the images. (Left panel) No voltage applied to the multichannel structure. (Right panel) A cluster with a width of seven microchannels filled with aqueous solution, activated by the applied voltage. The external valves (not visible) were open. (**B**) Filling/emptying curve of microchannels, for upward microchannel orientation. During the measurement, the external valves were open to maintain constant pressures in the communication channels. The voltage was swept at a rate of 10 V/s. The degree of microchannel filling has been determined by a measurement of the electrical capacitance. The right-hand scale gives the corresponding average level of aqueous solution in the microchannels. The symbols represent measured values, with dashed lines as guides to the eye. The solid lines represent calculations of the position of a meniscus in a microchannel, derived by balancing the ECP with the microchannel hydrophobicity and applied hydrostatic pressures. Parameters: $A = 0.12 \pm 0.01$ mm^2, $\ell = 1.29 \pm 0.05$ mm, $\varepsilon_r = 2.7$, $d = 11.5 \pm 0.5$ μm, coating hydrophobicity 57 mN/m for the filling curve, 49 mN/m for the emptying curve, mass density of the aqueous CsCl solution 1.11×10^3 kg/m^3, mass density of the decane oil 0.73×10^3 kg/m^3, a cluster of 270 microchannels. (**C**) Filling (V_{fill}) and emptying (V_{empty}) voltages as a function of the hydrostatic pressure applied to the meniscus. Closed symbols are the measured filling voltages, open symbols are the measured emptying voltages. The solid lines represent the calculated behavior.

voltage (Fig. 3B). The fluid level in the microchannels was determined by measuring the electrical capacitance between the aqueous solution and the wall electrodes. The capacitance gives a direct measure of the overlap between the aqueous solution and the microchannel walls. In the absence of an applied voltage, the capacitance is nearly zero because the menisci reside at the microchannel openings. The microchannels fill when the sum of ECP and applied hydrostatic pressures exceeds the hydrophobicity of the microchannel walls. Beyond the so-called filling voltage (V_{fill}, about 175 V in Fig. 3B) the measured capacitance increases steeply, indicating that the menisci enter the microchannels. For voltages above 210 V, the capacitance saturates because the menisci stop at the end of the aluminum electrodes in the microchannels. When the voltage is subsequently decreased, complete emptying of the microchannels is observed. The emptying voltage (V_{empty}) is somewhat lower than the filling voltage, a hysteresis due to movement of the fluid across imperfections on the microchannel walls. The solid lines represent calculations of the meniscus position in a microchannel, derived by balancing the ECP with the microchannel hydrophobicity and the applied hydrostatic pressures. The measured curves are broadened compared to the calculated curves due to parameter variations across the multichannel structure (mainly the cross-sectional area and insulator thickness). The filling and emptying voltage depend on the magnitude of the pressures in the communication channels. Figure 3C shows the voltages as a function of the hydrostatic pressure applied to the menisci. The filling and emptying voltage decrease when the applied pressure increases. The actuation voltages show a square-root dependence on the applied pressure, in agreement with Eq. 1.

For most applications, it is important to achieve insensitivity to gravitational forces. We observed equal curve shapes for all orientations with respect to gravity, with only a slight increase of hysteresis for orientations from sideways to inverted ($90° < \beta \leq 180°$) caused by the mass density difference of the fluids in the microchannels. The reversibility of actuation by ECP is outstanding: in our multichannel structures, we demonstrated completely reversible filling and emptying of microchannels for more than 200,000 cycles in all orientations with respect to gravity (*12*).

Finally, we studied the dynamic performance of ECP in a multichannel device. Figure 4 shows the operation with external valves closed. A symmetrical driving scheme was used, i.e., the activation of a cluster of microchannels was accompanied by the deactivation of another cluster of microchannels. We call this the "push-pull" mode of operation. Figure 4A shows an x-ray transmission image of the device in a switching state, the arrow indicating the direction of flow of the aqueous solution. A movie and animation can be found at (*13*). Figure 4B shows the time evolution of the fluid levels in the two respective clusters, demonstrating a velocity of 5 cm/s. The highest ECP-driven velocity that we have observed in the microchannels was 12 cm/s, measured with air instead of oil as the second fluid.

The phenomenon of ECP allows rapid and reversible fluid actuation in three-dimensional microchannel structures. ECP scales inversely with the microchannel radius, which makes it well suited for miniaturized devices. ECP does not involve mechanically moving parts, conferring advantages for reliability and integration density. The observed flow velocities of several centimeters per second are nearly two orders of magnitude higher than achieved by other nonmechanical electrofluidic actuation principles (*1, 2*). Because the operative electric fields are located close to the meniscus edge, it is an actuation principle with a high spatial resolution. ECP is of electrostatic origin, involving very low charge densities (of the order of 10^{-4} C/m^2) and very low displacement currents. In contrast to other electrofluidic actuation principles (*1, 2*), electrochemical reactions and electrolytic bubble formation are absent. Finally, because of the electrostatic nature of ECP, its energy consumption is zero at rest and very low during movement (a few microwatts per microchannel). The power efficiency of pumping by ECP is 50% (half of the energy is stored in the electrostatic field and half is resistively dissipated). For comparison, pumping by thermal bubble formation has a power efficiency well below 1%, mainly due to heat losses to the environment.

The concept of ECP is simple and powerful. It can be integrated into a variety of microfluidic fabrication technologies, for example, those based on thin plastic foils (*11*), on crystalline silicon (*14*), or on silicone rubbers (*15*). ECP is promising for applications that demand a high degree of switching reversibility, such as displays and optical switches. The fluidic control principle can also be applied to guide microparticles or microcapsules through three-dimensional networks of channels. Advanced flow architectures are possible, for example, based on push-pull geometries. Sustainable fluid transport can be achieved by proper sequencing of voltages. Finally, secondary fluids can be actuated via membranes or flexible channel walls to avoid chemical interferences. This will enable ECP to become an integrated engine for future (bio) chemical microanalysis and microsynthesis.

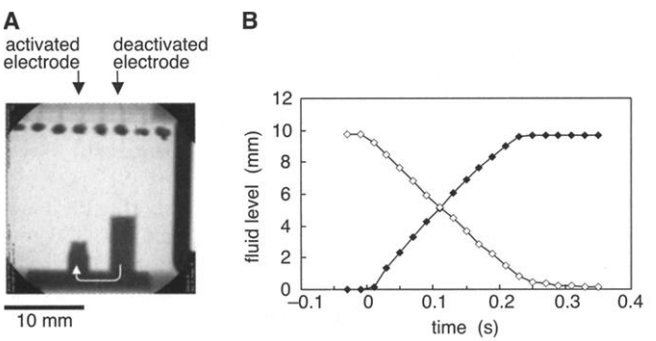

Fig. 4. (**A**) Simultaneous activation and deactivation of microchannels. The figure shows a transmission x-ray image as in Fig. 3A. The arrow indicates the direction of movement of the aqueous solution. (**B**) Measured fluid level as a function of time, for filling (closed symbols) as well as emptying (open symbols) microchannels. At $t = 0$, filling was induced by applying a voltage step from 0 to −237 V and emptying by a step from −237 to 0 V. The fluid level was determined from equal gray-level contours in x-ray images.

References and Notes

1. B. S. Gallardo *et al.*, *Science* **283**, 57 (1999).
2. R. B. M. Schasfoort, S. Schlautmann, J. Hendrikse, A. van den Berg, *Science* **286**, 942 (1999).
3. E. Colgate, H. Matsumoto, *J. Vac. Sci. Technol. A* **8**, 3625 (1990).
4. B. Berge, *C. R. Acad. Sci. Paris Ser. II* **317**, 157 (1993).
5. H. J. J. Verheijen, M. W. J. Prins, *Langmuir* **15**, 6616 (1999).
6. B. Janocha, H. Bauser, C. Oehr, H. Brunner, W. Göpel, *Langmuir* **16**, 3349 (2000).
7. M. G. Pollack, R. B. Fair, A. D. Shenderov, *Appl. Phys. Lett.* **77**, 1725 (2000).
8. G. Lippmann, *Ann. Chim. Phys.* **5**, 494 (1875).
9. Note that our approach is different from electrocapillarity in the classical mercury/electrolyte system (*8, 16, 17*). In these studies, all fluids are electrically conducting and a voltage modifies the fluid/fluid instead of the fluid/solid interfacial tension. Although fluid velocities of centimeters per second can be reached (*17*), the mercury/electrolyte system is not suitable for multichannel networks because of the high electrical conductances of the fluids, causing high currents and cross-talk between neighboring channels and cells. Furthermore, because of large mass density differences, the mercury/electrolyte system is very sensitive to gravitational forces.
10. The term "electrocapillary pressure" refers to the pressure generated in a microchannel by electrocapillary effects. We find this term more appropriate to describe our experiments than, for example, "competitive electrowetting (*6*) pressure" or "electrowetting-based microactuation" (*3*). One reason is that (competitive) electrowetting is centered around contact angles and (competitive) wettability. Contact angles are important and measurable for droplets and planar geometries. In microchannels of arbitrary shape, it is the voltage-dependent meniscus pressure rather than the local contact angle that is important and measurable. An obvious difference between "electrocapillary pressure" and "electrowetting" exists for material systems with a contact angle of 0° (completely wetting) or 180° (completely nonwetting). These systems do not electrowet (i.e., do not show a dependence of contact angle on applied voltage) but do show an ECP (i.e., a voltage-dependent meniscus pressure in a microchannel).
11. M. W. J. Prins, J. W. Weekamp, J. B. Giesbers, *J. Micromech. Microeng.* **9**, 362 (1999).

12. The choice of aqueous solution has an influence on the long-term reversibility of filling/emptying cycles. We tested aqueous solutions with a pH between 1 and 10, with a variety of dissolved salts (Na, K, Cs, Sm, Cl, SO_4, NO_3, acetate etc.) and also with dyes added to the aqueous solution (e.g., black ink and Cresol Red). In every case, tests always exceeded 1000 filling/emptying cycles. Our longest test involved 200,000 filling/emptying cycles with a CsCl solution, showing a perfectly reversible behavior. Note that surface-active components in the solution can affect the hydrophobicity of the microchannel walls; this can be compensated for by a change of the hydrostatic pressure in the communication channels.
13. Supplementary material is available at www.sciencemag.org/cgi/content/full/291/5502/277/DC1.
14. Special issue on silicon micromachining, *Proc. IEEE* **86**, 1536 (1998).
15. M. A. Unger, H.-P. Chou, T. Thorsen, A. Scherer, S. R. Quake, *Science* **288**, 113 (2000).
16. A. W. Adamsom, A. P. Gast, *Physical Chemistry of Surfaces* (Wiley, New York, 1997).
17. J. Lee, C.-J. Kim, *IEEE J. Microelectromech. Syst.* **9**, 171 (2000).
18. We thank B. Giesbers, B. van Nunen, D. van den Broek, C. Nederpelt, and W. van den Meijdenberg for technical support. The following students contributed to the project: K. Guillaume, A. Kemmeren, M. van Schijndel, L. Willems van Beveren, T. van Woudenbergh, J. van't Westende, J. Crawford, D. Damen, L. Thibaud, and D. McGeoch. We thank J. Feenstra, R. Hayes, and E. Bosch for helpful discussions.

31 August 2000; accepted 28 November 2000

Proximity-Induced Superconductivity in DNA

A. Yu. Kasumov,[1,2]* M. Kociak,[1] S. Guéron,[1] B. Reulet,[1] V. T. Volkov,[2] D. V. Klinov,[3] H. Bouchiat[1]

Conductivity measurements on double-stranded DNA molecules deposited by a combing process across a submicron slit between rhenium/carbon metallic contacts reveal conduction to be ohmic between room temperature and 1 kelvin. The resistance per molecule is less than 100 kilohm and varies weakly with temperature. Below the superconducting transition temperature (1 kelvin) of the contacts, proximity-induced superconductivity is observed. These results imply that DNA molecules can be conducting down to millikelvin temperature and that phase coherence is maintained over several hundred nanometers.

The desire to use molecules as the ultimate building blocks of electronic circuits motivates the quest to understand transport in molecular wires. However, most molecules with delocalized electronic orbitals undergo a structural Peierls transition to an insulating state at low temperature (*1*). Few systems are exceptions to this rule, with carbon nanotubes being one of them (*2*). The situation of DNA molecules is controversial. Optical experiments have indicated the possibility of charge transfer in DNA molecules (*3*). As for transport measurements, some indicate that DNA molecules could be conducting (*4*, *5*), and others indicate that they are insulating (*6*, *7*). Fink *et al.* (*5*) found that a small bundle of DNA molecules suspended across a hole in a metallic grid had an ohmic behavior (linear IV curve). They found a resistance on the order of 1 megohm for a 1-μm-long sample. In contrast, Porath *et al.* (*7*) measured a single 10-nm-long DNA molecule that had been electrostatically trapped between electrodes 8 nm apart and found a nonlinear current voltage characteristic, with an insulating gap of several hundred millivolts.

Motivated by this puzzle, we performed transport experiments on DNA molecules connected to superconducting electrodes 0.5 μm apart. We observed a conducting behavior, with signs of proximity-induced superconductivity below the superconducting transition temperature of the electrodes. The proximity effect (PE)—the penetration of superconducting correlations in a nonsuperconducting (normal) conductor connected to it—has been extensively measured in metallic multilayers, mesoscopic wires made of noble metals (*8*, *9*), and more recently in carbon nanotubes (*10*). Observing a PE in DNA molecules implies that these molecules are conducting, that their phase coherence length is on the order of the length of the molecules, and that they form a low-resistance contact with the superconducting electrodes.

The experimental system consisted of double-stranded 16-μm-long λ-DNA molecules connecting two superconducting rhenium/carbon (Re/C) electrodes, deposited by sputtering on a freshly cleaved mica substrate. The Re film was 2 nm thick. The same nominal thickness of C did not produce a smooth film but rather a "forest" of individual fibers up to 40 nm tall (Fig. 1). The resistance of the Re/C bilayer was 100 ohm per square and underwent a superconducting transition around 1 K. The chosen thickness of the Re film was intended to minimize kinks in the DNA molecules at the edges of the metallic pads, because such kinks could hinder electronic transport from the contacts through the molecule. The deposited Re/C film was cut by a focused laser beam (Fig. 1A) in order to prepare six structures for transport measurements. Each structure consisted of a double submicron slit that separated the Re/C film into two broad electrodes. The resistance of the structures was more than 1 gigohm and decreased to several kilohm after deposition of DNA molecules.

In order to obtain aligned DNA molecules across the submicron gaps, we first glow-discharged the Re/C-covered mica substrate in the presence of pentylamine vapor, in order to promote adhesion (*11*). We then combed the DNA molecules using a continuous flow of DNA solution (*12*–*14*). After deposition, the samples were imaged with an atomic force microscope (AFM). The density of deposited DNA molecules depended on the duration of deposition. We prepared two samples with different estimated linear densities of DNAs perpendicular to the flow: 3000 and 6000 cm^{-1}, corresponding, respectively, to 4 and 10 min of adsorption time. We estimate that about 100 and 200 DNA molecules bridged the two electrodes in these two respective samples, yielding a total resistance of 3 to 4 kilohm and 2 to 3 kilohm, respectively, and corresponding to an average resistance of about 300 kilohm per DNA molecule. However, this number is probably overestimated, because only a fraction of the combed molecules is likely to be in good contact with the electrodes. We also checked that the resistance of the structures remained greater than 1 gigohm after treatment in a buffer solution (without DNA) flow. After DNA deposition, we attempted to isolate a single DNA molecule by destroying the other molecules with a low-power focused laser beam. To this end, we scanned the focused laser beam at low power (the beam diameter was about 1 μm, with power about 10 times less than used for cutting of the Re/C film) along the slit, except for a window that was left unetched. Scanning along the gap destroyed DNA molecules connecting the two electrodes and increased the resistance of the structure.

We present low-temperature transport measurements on three such structures: sample DNA1, with a 30-μm-wide unetched window, contained approximately 10 combed molecules as estimated from AFM observations; sample DNA2, with a 120-μm-wide window, had about 40 combed DNAs; and sample DNA3 had only a few molecules (probably two or three). The room tempera-

[1]Laboratoire de Physique des Solides, Associé au CNRS, Bât 510, Université Paris-Sud, 91405, Orsay, France. [2]Institute of Microelectronics Technology and High Purity Materials, Russian Academy of Sciences, Chernogolovka 142432 Moscow Region, Russia. [3]Shemyakin-Ovchinnikov Institute of Bioorganic Chemistry, Russian Academy of Sciences, Miklukho-Maklaya 16/10, Moscow 117871, Russia.

*Present address: Starlab, La tour de Freins, 555 rue Engeland 1180 Uclle, Brussels, Belgium.